EPR Investigation of Synthetic, Doped FeS_2 and RuS_2 Single Crystals.

M. Schuler, J. Dahlem, and D. Siebert

Institut für Physikalische Chemie, Albert-Ludwigs-Universität, Albertstr. 23a, 79104 Freiburg i. Br.

Z. Naturforsch. **50 a,** 1159–1164 (1995); received October 17, 1995

Synthetic FeS_2 and RuS_2 single crystals were prepared by the flux method using $PbCl_2$, bismut, and tellurium as different solvents. FeS_2 and some RuS_2 samples were doped with elementary vanadium, other RuS_2 crystals with manganese and nickel. The EPR spectra revealed Mn^{2+} in the low-spin state and Ni^{2+}. The lineshape of the Mn sextet turned out to be asymmetrical. In some RuS_2 samples we detected an isotropic structureless rather narrow signal with a linewidth down to 0.05 mT and attributed it to the conductivity. Its lineshape becomes symmetrical and Lorentzian by grinding the samples to a polycrystalline powder. The EPR parameters of appropriate spin-Hamiltonians were determined. The intensities of the allowed and forbidden lines depended very differently on the microwave power due to different degrees of saturation.

Key words: FeS_2, RuS_2, EPR, paramagnetic ions, conductivity.

1. Introduction

RuS_2 and FeS_2 belong to the family of transition-metal dichalcogenides crystallizing in the pyrite structure. There is an increasing interest in synthetic pyrite (cubic FeS_2) with regard to its electrical conductivity and photovoltaic properties [1]. In electrochemical investigations the ruthenium compounds have been attractive as electrode or photoelectrode materials because of their catalytic properties [2] and favourable stability [3].

Formerly we detected and investigated several paramagnetic species in single crystals of FeS_2 [4, 5, 6] and in RuS_2 [7]. Yu et al. performed similar EPR measurements with FeS_2 [8] that agree with ours essentially.

Furthermore they studied paramagnetic species of electronic spin S = 1/2 in undoped, as-grown RuS_2 single crystals [9] and in solid solutions $Ru(S_{1-x}Se_x)_2$ [10]. They reported on Mn^{2+} in the low spin state in RuS_2 [11], determined a $g_\perp$ of 2.135 and a hyperfine constant of 0.0081 cm^{-1}. Tsay et al. [12] prepared single crystals of $Ru_xFe_{1-x}S_2$ by chemical vapour transport and flux methods and proposed S^- associated with an S vacancy. In this paper we report on an EPR study of several new, paramagnetic centers in FeS_2 and RuS_2, produced by extra doping.

Reprint requests to Prof. Dr. D. Siebert.

2. The Crystals

2.1. FeS_2

V-doped crystals were obtained from a $PbCl_2$ melt. We prepared mixtures of FeS_2 powder and $PbCl_2$ 99.999 % in a ratio of 1:12 by weight together with 10 mol% vanadium powder in evacuated and sealed quartz ampoules. These ampoules were heated to 850 °C and then slowly cooled at a rate of 2 °C/h down to 500 °C. To separate the FeS_2 crystals from the solid melt, $PbCl_2$ was dissolved in 16 % HCl and 2M NaOH. Single crystals up to 4 mm edge length could be obtained.

2.2. RuS_2

The crystals doped with elementary vanadium (10 mol%) or nickel (10 mol%) were grown from solutions with bismut as a solvent [13], and the Mn-doped crystals were obtained from a Te melt [14]. We prepared mixtures of RuS_2 powder and bismut (99.999 %) in a ratio of 1:40 by weight, and for the Mn-doped crystals mixtures of RuS_2 powder and tellurium in a ratio of 1:32 by weight together with 10 mol% manganese powder in evacuated and sealed quartz ampoules. These ampoules were heated to 1040 °C and then slowly cooled at a rate of 2 °C/h down to 500 °C and at a rate of 1 °C/h down to 550 °C,

0932-0784 / 95 / 1200-1159 $ 06.00

respectively. To separate the RuS_2 crystals from the solid melt, bismut was dissolved in 30 % HNO_3, and the solid tellurium melt in aqua regia. Single crystals up to 4 mm edge length could be obtained.

3. EPR Spectra and Analysis

3.1. Experimental

Our EPR measurements were performed at 78 K with a conventional Varian X-band spectrometer and a standard TE_{102}-cavity with 100 kc modulation. At room temperature the cavity loading was too high for the crystal used, because of their conductivity. The X-band frequency was measured with a frequency counter, the magnetic field by a Bruker NMR magnetometer. The crystal structure of FeS_2 and RuS_2 is the well known pyrite structure. The space group is $P2_1/a\bar{3}$, the cation sites and the sites of the S_2 dumb-bells have the local symmetry $\bar{3}$. For those investigated centers that were orientational dependent, we observed four lines for each transition. This site splitting agreed with the local symmetry $\bar{3}$, the $\bar{3}$ axes being parallel to the four different $\langle 111 \rangle$ directions. In consequence the signals were attributed to substitutional centers.

It was convenient to use the site splitting for an accurate setting of the crystal orientation, especially for $\boldsymbol{B}_0$ parallel to $\langle 100 \rangle$, $\langle 110 \rangle$ and $\langle 111 \rangle$, where signals coincide. For Θ, the angle between center axis and magnetic field, we realized the values 54.7°, 35.3° and 90.0°, 0.0° and 70.5°, respectively [4]. Furthermore we studied the EPR lines qualitatively at different microwave powers to get some information about the saturation behaviour of the centers.

3.2. Analysis of the Spectra

The EPR parameters were obtained from the spectra by a computer fitting procedure [4]. This program compared experimental and calculated magnetic fields for an assumed set of EPR parameters. The resonance fields were calculated by means of exact numerical diagonalization of the spin-Hamiltonian matrices. For each transition the quantum mechanical transition probability

$$|\mu_{ij}|^2 \propto | < i \,|\mathcal{H}_1/\beta B_1|\, j > |^2 \qquad (1)$$

with

$$\begin{aligned}(\mathcal{H}_1/\beta B_1) \;=\; & (\cos\theta\cos\phi\cos\chi - \sin\phi\sin\chi)g_x S_x \\ & + (\cos\theta\sin\phi\cos\chi - \cos\phi\sin\chi)g_y S_y \\ & -(\sin\theta\cos\chi)g_z S_z. \qquad (2)\end{aligned}$$

was calculated from the diagonalization procedure. $\mathcal{H}_1$ denotes the Zeeman operator due to the magnetic field B_1 of the microwave [4].

3.3. V-doped Crystals

In both RuS_2 and FeS_2 we found a distinct hyperfine structure (HFS) corresponding to a nuclear spin $I = 7/2$ and several small lines within the HFS (Figure 1). The signal octet of the resonance varied from about 0.16 to 0.32 Tesla, characteristic for $S = 3/2$ in a strong axial field. Furthermore we were able to detect the signals expected at higher fields near 0.5 Tesla for $\boldsymbol{B}_0 \| z$, and 0.7 Tesla for $\boldsymbol{B}_0 \perp z$ (cf. Cr^{3+} in RuS_2, Fig. 3 in [7]).

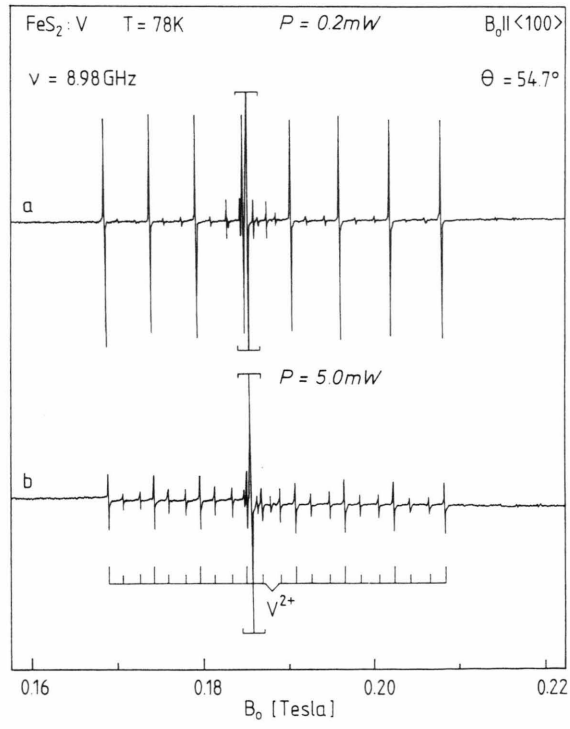

Fig. 1. EPR resonances of V^{2+} in FeS_2 at 78 K for $\boldsymbol{B}_0 \| \langle 100 \rangle$; Detection at different microwave power: (a) P = 0.2 mW, (b) P = 5.0 mW. The strong line and the hyperfine quartet correspond to Cr^{3+} [5].

Table 1. EPR parameters for RuS_2 and for FeS_2; b_2^0 in cm^{-1}, $A_{||}$, $A_\perp$, A_0, $T_{||}$ in 10^{-4} cm^{-1}; $*$: parameters are determined in this work.

	$g_{||}$	$g_\perp$	b_2^0	$A_{||}$	$A_\perp$	A_0	$T_{||}$	Ref.
RuS_2								
V^{2+}	2.0040	2.0000	0.407	47.9	52.6	—	—	*
Mn^{2+}	2.0185	2.1435	—	– 6.8	81.1	51.8	–58.6	*
Ni^{2+}	2.1053	2.1122	(–)1.729	—	—	—	—	*
FeS_2								
V^{2+}	2.0101	2.0035	0.3601	44.1	48.3	—	—	*
Mn^{2+}	2.0377	2.1490	—	– 8.7	75.1	47.2	–55.9	[4]
Ni^{2+}	2.0921	2.0893	(–)1.208	15.5	13.0	—	—	[5]

The received data can be described satisfactorilly with the specialized spin-Hamiltonian for electronic spin $S = 3/2$ and the above nuclear spin [5]:

$$\mathcal{H} = g_{||}\beta B_z S_z + (1/2)g_\perp\beta(B_+S_- + B_-S_+) + (b_2^0/3)(3S_z^2 - S(S+1)) + A_{||}S_zI_z + (1/2)A_\perp(S_+I_- + S_-I_+). \quad (3)$$

The strong lines in Fig. 1 represent the allowed transitions with $\Delta m = 0$ and the small lines the forbidden transitions with $\Delta m = 1$. The EPR spectrum of V-doped FeS_2 is shown in Fig. 1 for $\Theta = 54.7^o$. The stick diagram shows an excellent agreement of the experimental and theoretical spectrum. This is representative also for the other characteristic angles. The EPR parameters are listed in Table 1. The hyperfine parameters $A_{||}$ and $A_\perp$ were determined from the resonances $\boldsymbol{B}_0||z$ and $\boldsymbol{B}_0 \perp z$, correspondingly.

3.4. Mn-doped Crystals

The EPR spectrum is presented in Fig. 2 for $B_0||\langle 111\rangle$. There is a sextet for $\theta = 0°$ and another one for $\theta = 70.5°$ with threefold intensity. As in similar investigations on FeS_2 [4] we analyzed the spectrum by the spezialized spin-Hamiltonian for an electron spin $S = 1/2$ and nuclear spin $I = 5/2$ of the ^{55}Mn nucleus for axial symmetry:

$$\mathcal{H} = g_{||}\beta B_z S_z + (1/2)g_\perp\beta(B_+S_- + B_-S_+) + A_{||}S_zI_z + (1/2)A_\perp(S_+I_- + S_-I_+). \quad (4)$$

The good agreement of the calculated fields at resonance with the experimental values in Fig. 3 proves, that Mn^{2+} is in the low-spin state in RuS_2 as in FeS_2.

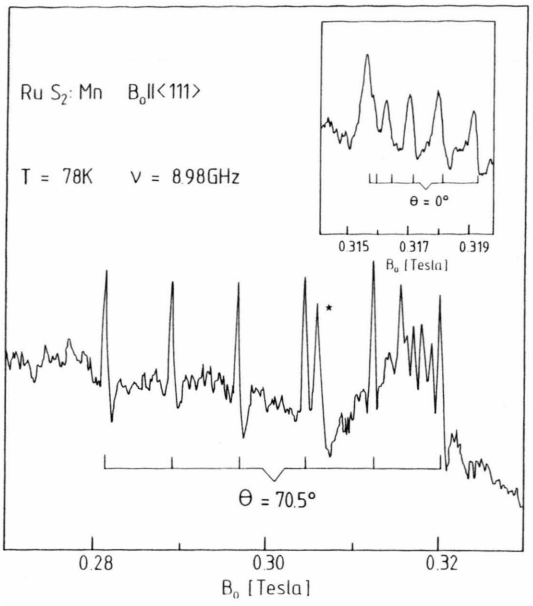

Fig. 2. Experimental and theoretical spectrum of Mn^{2+} in RuS_2 at 78 K for $\boldsymbol{B}_0||\langle 111\rangle$; $\star$ denotes an isotropic signal which originates from delocalized electrons.

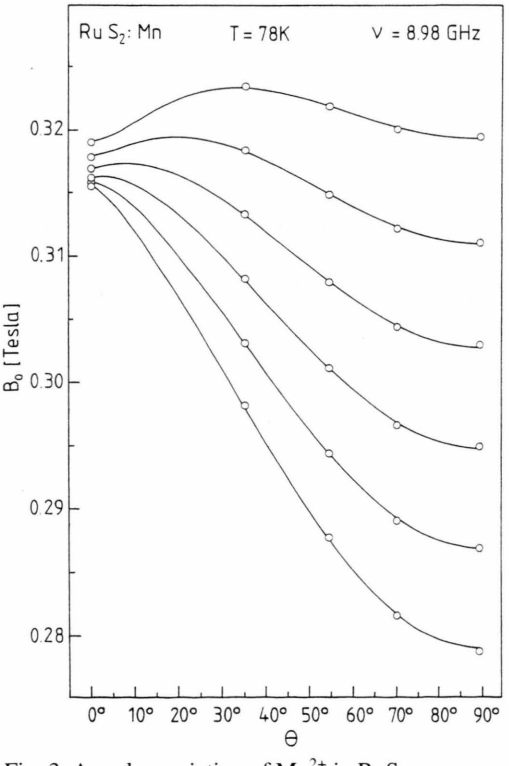

Fig. 3. Angular variation of Mn^{2+} in RuS_2; o o o experimental, —— theoretical values.

Furthermore we observed an asymmetric lineshape of the signals.

3.5. Ni-doped Crystals

In Ni-doped RuS_2 we found an EPR signal without HFS which varied between 0.19 and 0.79 mT, and its intensity decreased from higher to lower magnetic fields. This is characteristic for a transition that becomes forbidden between the pure states $|-1\rangle$ and $|1\rangle$, i.e. the spin has to be integer. The observation is similar to that of Ni^{2+} in FeS_2 [5]. Therefore we analyzed the different resonance lines with the spin-Hamiltonian (see (3)) for electronic spin $S = 1$ and nuclear spin $I = 0$ and found a very good agreement with the experimental values as shown in Figure 4. The determined EPR-parameters are listed in Table 1.

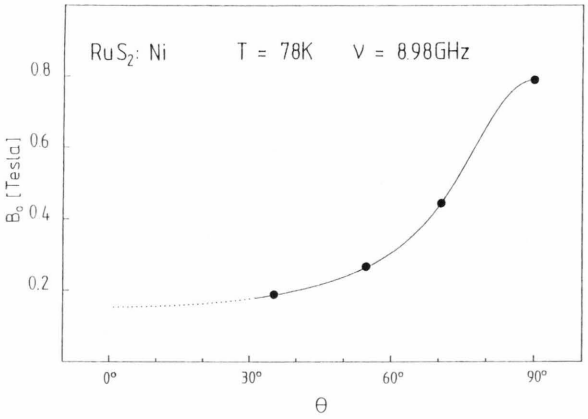

Fig. 4. Angular variation of Ni^{2+} in RuS_2; • • • experimental values; ——, · · · theoretical values; · · · small transition probability.

3.6. Isotropic EPR Signal

The surplus line (marked with ⋆ in Fig. 2) had been found in several different doped single crystals. It was detected as a rather narrow isotropic EPR line with $g = 2.069 \pm 0.001$, linewidth down to 0.05 mT, and without HFS. By grinding some samples to polycrystalline powder the lineshape changed to a symmetric one (Figures 5a and b). Following [17] we analyzed the signal with the function that describes the first derivative of a Lorentzian lineshape

$$Y'_L = \frac{16 y'_m [(B - B_0)/\frac{1}{2}\Delta B_{pp}]}{[3 + \{(B - B_0)/\frac{1}{2}\Delta B_{pp}\}^2]^2}. \qquad (5)$$

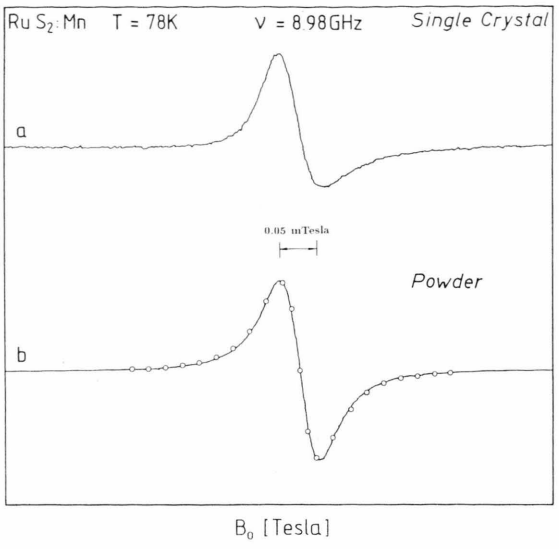

Fig. 5. Isotropic EPR resonance in RuS_2 at $g = 2.069 \pm 0.001$; (a) single crystal, (b) polycrystalline powder; o o o theoretical values from Lorentzian lineshape function.

y'_m denotes the line amplitude, ΔB_{pp} the peak-to-peak linewidth. The good agreement of the calculated values (marked by o) with the measured line is shown in Figure 5b.

4. Discussion

4.1. FeS_2: V and RuS_2: V

Similar to previous investigations we found that the g-value for V^{2+} is greater than the free electron value, g_e, although the shell of d-electrons is less than half-filled. We conclude that there is a strong covalent bond in FeS_2 and in RuS_2 . But in RuS_2 the g-values are nearer to g_e and the values for $A_{||}$ and $A_\perp$ are greater than in FeS_2. According to this, the covalency of the sulfur bond in RuS_2 is smaller.

As V^{2+} and Cr^{3+} are isoelectronic with the configuration $(Ar)3d^3$, we determined the following ratios (see Table 1):

$$\begin{aligned} A_{||}(Cr^{3+})/A_{||}(V^{2+}) &= 0.284 \text{ for } FeS_2, \\ &= 0.260 \text{ for } RuS_2; \\ A_\perp(Cr^{3+})/A_\perp(V^{2+}) &= 0.277 \text{ for } FeS_2, \\ &= 0.262 \text{ for } RuS_2. \end{aligned}$$

This has to be compared with $|g_N|(Cr^{3+})/|g_N|(V^{2+}) = 0.214$. The result shows an approximate agreement between the ratios of HF constants and the ratios of the nuclear magnetic moments, i. e. the ratios of the

g_N values, indicating that the electronic structures of the different paramagnetic centers are similar.

The dependence of the EPR signals from the microwave power originates from a well known saturation phenomenon described in [17, 18]. With increasing value of microwave power the intensities of the strong lines were quenched and the small lines grew stronger. The mechanism can be explained qualitatively with relation for the power absorbed by the spin system

$$\frac{dW}{dt} = \frac{\Delta N h\nu w_{ij}}{1 + 2w_{ij}\tau_1}, \tag{6}$$

were τ_1 denotes the spin-lattice relaxation time, $\Delta N = N_i - N_j$ the population difference between an upper level j and a lower level i of a simple two-level system in the equilibrium state. For the number of transitions between the energy levels, which are induced by an oscillatory field of amplitude B_1 and angular frequency ω, is

$$w_{ij} = \frac{\pi B_1^2}{2\hbar^2}|\mu_{ij}|f(\omega). \tag{7}$$

For linear detectors the absorption signal detected experimentally is proportional to the out of phase magnetization component $B_1\chi''$, and one obtains

$$B_1\chi'' = \frac{2\hbar|\mu_{ij}|^2 B_1\, \Delta N\, C(\omega)}{1 + 2C(\omega)B_1^2|\mu_{ij}|\tau_1}, \tag{8}$$

where $C(\omega)$ describes the lineshape. Referring to (8) the strong lines with high transition probabilities $|\mu_{ij}|$ can be saturated earlier than the weaker lines according to lower transition probabilities for the latters (see Figures 1a and b). This phenomenon had been found by us in RuS_2 as well, but at higher microwave power because of additionally inhomogenous broadening effects.

4.2. *RuS_2: Mn*

Compared with results from Mn-doped FeS_2 crystals we assign the spectrum of Fig. 2 to Mn^{2+} in the low-spin state on a cation site in RuS_2, as assumed for Ru^{2+}. Yu et al. [11] reported a $g_{||} < 0.5$ and a $g_\perp = 2.135$ from a powder spectrum. Now we were able to find a whole angle variation and also it was possible to determine the complete set of EPR parameters (see Table 1). The value for $A_\perp = 0.0081\ cm^{-1}$ of Yu et al. [11] is in agreement with our measurements.

Following [16] the hyperfine interaction tensor **A** is decomposed as usually in an isotropic part $\mathbf{A}_0$ with the principal value A_0 and a traceless tensor **T** with principal values $T_\perp$ and $T_{||} = -2T_\perp$ (see Table 1). For $T_{||}$ a simple one electron model predicts $T_{||} = -\frac{2}{7}g\beta g_N\beta_N\langle r^3\rangle$ [6, 15]. After the tables of atomic parameters [15] we get $T_{||} = -160$ MHz and experimentally -175 MHz corresponding to $-0.00586\ cm^{-1}$. With regard to the crude approximation that does not consider the orbitals of the ligands, the agreement is quite good.

For the isotropic part A_0 we obtained $0.00518\ cm^{-1}$. As in FeS_2 we explain this by a very small admixture of 4s states that is higher in RuS_2 compared to FeS_2. This may be due to the higher lattice constant [19, 20] and the 4s electrons could claim more room. According to Koh and Miller [15] a pure 4s electron centered on Mn^{2+} would produce an isotropic hyperfine constant of 4731 MHz compared to only 155.3 MHz from Table 1.

The asymmetry of the EPR signals is a consequence of the high conductivity of the crystals. If the skin depth is much smaller than the thickness of the crystals, the observed line is a mixture of a dispersion and an absorption curve [21].

4.3. *RuS_2: Ni*

Because of doping RuS_2 with elementary nickel and due to the spin value $S = 1$ we assigned Ni^{2+} on *Ru* site to the observed EPR resonance. The result is similar to that of Ni^{2+} in FeS_2 [5]. We were not able to measure the weak HFS of the isotope ^{61}Ni with a nuclear spin $I = 3/2$ because of the broadened lines due to interactions with the nearest Ru neighbours ($I = 5/2$ for ^{99}Ru (12 %) and ^{101}Ru (17 %)). The g values of Ni^{2+} in RuS_2 are greater than the free electron value, as it should be for more than five d electrons. Compared with FeS_2, they are smaller than usually as well, but nearer to the values (2.20-2.25) obtained in many oxides. The result indicates that the covalency of the sulfur bond in RuS_2 is smaller than in FeS_2, in accordance with previous discussions of Cr^{3+} [7] or V^{2+} in the above section.

4.4. *Isotropic Resonance*

The detection of an isotropic single EPR line is reported by Yu et al. [10]. They studied a paramagnetic center with an electronic spin $S = 1/2$ and

found an anisotropic g-factor. After recrystallization from small crystals without adding an extra amount of sulfur to the starting material, the anisotropy of the g-factor was much reduced. This observation had been confirmed after heating of some crystals in sealed quartz ampoules at 1100°C for 5 days. Now the EPR spectrum consisted of an isotropic line with a g value of 2.068 ± 0.001 which agrees with ours very well. But the line breadths between 0.89 and 1.7 mT of their signals were greater than that of our isotropic resonance with only 0.05 mT linewidth.

Yu et al. concluded that the isotropic line originates from delocalized electrons as arising from an overlap of the wave functions due to the sulfur deficiency. They assumed the formation of a narrow band within the gap of RuS_2 in agreement with Birkholz et al. [22]. The Lorentzian line shape, demonstrated by us in Fig. 5b, is characteristic for delocalized electrons. The conclusion is confirmed by the fact of high cavity loading at room temperature.

Acknowledgements

Financial support of the "Deutsche Forschungsgemeinschaft" and the "Fonds der Chemischen Industrie" is gratefully acknowledged.

[1] R. Schieck, A. Hartmann, S. Fiechter, R. Könenkamp, and H. Wetzel, J. Mater. Res. **5**, 1567 (1990).
[2] R. R. Chianelli, T. A. Pecoraro, T. R. Halbert, W. H. Pan, and E. J. Stiefel, J. Catal. **86**, 226 (1984).
[3] H. Ezzaouîa, and R. Heindl, J. Electroanal. Chem. **165**, 155 (1984).
[4] D. Siebert, J. Dahlem, S. Fiechter, and A. Hartmann, Z. Naturforsch. **44a**, 59 (1989).
[5] D. Siebert, R. Miller, S. Fiechter, P. Dulski, and A. Hartmann, Z. Naturforsch. **45a**, 1267 (1990).
[6] D. Siebert, J. Dahlem, S. Fiechter, and R. Miller, phys. stat. sol. (b) **171**, K93 (1992).
[7] M. Schuler and D. Siebert, phys. stat. sol. (b) **188**, K25 (1995).
[8] J. T. Yu, Y. S. Huang, and M. Y. Tsay, J. Appl. Phys. **75**, 10 (1994).
[9] J. T. Yu, S. S. Lin, and Y. S. Huang, J. Appl. Phys. **65**, 4230 (1989).
[10] J. T. Yu, S. S. Lin, and Y. S. Huang, J. Appl. Phys. **68**, 1796 (1990).
[11] J. T. Yu, Y. S. Huang, and S. S. Lin, J. Phys.: Condens. Matter **2**, 5587 (1990).
[12] M. Y. Tsay, S. H. Chen, C. S. Chen, and Y. S. Huang, J. Crystal Growth **144**, 91 (1994).
[13] S. Fiechter and H. M. Kühne, J. Crystal Growth **83**, 517 (1987).
[14] H. Ezzauîa, R. Heindl, and J. Loriers, J. Mat. Science Letters **3**, 625 (1984).
[15] A. K. Koh and D. J. Miller, Atomic Data and Nuclear Data Tables **33**, 235 (1985).
[16] A. Carrington and A. D. McLachlan, Introduction to Magnetic Resonance, Harper & Row, New York, p. 155 and 105 (1969).
[17] C. P. Poole, Jr., Electron Spin Resonance, Wiley & Sons, New York, London, Sidney, p. 799 (1967).
[18] A. Abragam, and B. Bleaney, Electron Paramagnetic Resonance of Transition Ions, 1970, p. 60 and 119.
[19] J. C. Marianze, Phys. Rev. **96**, 593 (1954).
[20] F. Hulliger, Nature, London **200,** 1064 (1963).
[21] J. Owen, M. E. Browne, V. Arp, and A. F. Kip, J. Phys Chem Solids **2**, 85 (1957).
[22] M. Birkholz, A. Hartmann, S. Fiechter, and H. Tributsch, E. C. Photovoltaic Sol. Energy Conf., Proc. Int. Conf., 10th, 96 (1991).